Journal of Geodesy (2003) 77: 411–422
DOI 10.1007/s00190-003-0326-5

Journal of Geodesy

GPS network monitors the Arabia-Eurasia collision deformation in Iran

F. Nilforoushan[1], F. Masson[2], P. Vernant[2], C. Vigny[3], J. Martinod[4], M. Abbassi[5], H. Nankali[1], D. Hatzfeld[4], R. Bayer[2], F. Tavakoli[1], A. Ashtiani[5], E. Doerflinger[2], M. Daignières[2] P. Collard[2], J. Chéry[2]

[1] Geodynamic Department, National Cartographic Centre, PO Box 13185–1684, Meraj Ave, Tehran, Iran
e-mail: f-nilf@ncc.neda.net.ir; Tel.: +98 21 6004625; Fax: +98 21 6001972
[2] Laboratoire Dynamique de la Lithosphère, Université Montpellier II – CNRS, Pl. E. Bataillon, 34095 Montpellier Cedex 05, France
e-mail: fmasson@dstu.univ-montp2.fr
[3] Laboratoire de Géologie, Ecole Normale Supérieure – CNRS, 24 rue Lhomond, 75231 Paris Cedex 05, France
[4] Laboratoire de Géophysique Interne et Tectonophysique, Université Joseph Fourrier Grenoble – CNRS, BP 53, 38041 Grenoble Cedex 9, France
[5] International Institute of Earthquake Engineering and Seismology, Farmanieh, Dibaji, Arghavan St., No. 27, 19531 Tehran, Iran

Received: 22 July 2002 / Accepted: 26 March 2003

Abstract. The rate of crustal deformation in Iran due to the Arabia–Eurasia collision is estimated. The results are based on new global positioning system (GPS) data. In order to address the problem of the distribution of the deformation in Iran, Iranian and French research organizations have carried out the first large-scale GPS survey of Iran. A GPS network of 28 sites (25 in Iran, two in Oman and one in Uzbekistan) has been installed and surveyed twice, in September 1999 and October 2001. Each site has been surveyed for a minimum observation of 4 days. GPS data processing has been done using the GAMIT-GLOBK software package. The solution displays horizontal repeatabilities of about 1.2 mm in 1999 and 2001. The resulting velocities allow us to constrain the kinematics of the Iranian tectonic blocks. These velocities are given in ITRF2000 and also relative to Eurasia. This last kinematic model demonstrates that (1) the north–south shortening from Arabia to Eurasia is 2–2.5 cm/year, less than previously estimated, and (2) the transition from subduction (Makran) to collision (Zagros) is very sharp and governs the different styles of deformation observed in Iran. In the eastern part of Iran, most of the shortening is accommodated in the Gulf of Oman, while in the western part the shortening is more distributed from south to north. The large faults surrounding the Lut block accommodate most of the subduction–collision transition.

Keywords: Plate collision – Deformation – Global positioning system – Iran – Alpine-Himalayan collision zone

Correspondence to: F. Masson

1 Introduction

The present tectonics of Iran results from the north–south convergence between relatively undeformed shield areas to the southwest (Arabia) and northeast (Eurasia). The global plate motion model NUVEL-1 A (DeMets et al. 1990, 1994) predicts a convergence rate of 3–3.5 cm/year. The deformation of Iran involves intracontinental shortening, except along its southeastern margin (Makran) where the Oman oceanic lithosphere subducts northward under southeast Iran (Fig. 1). Within Iran, most of the deformation is probably accommodated in the major belts (Zagros, Alborz, Kopet-Dag) and along large strike-slip faults which surround blocks (the Central Iranian Desert, the Lut block and the southern Caspian Sea) with moderate relief and seismicity (Jackson and McKenzie 1984; Berberian and Yeats 1999).

The precise distribution of the deformation between these tectonic structures is unclear. Modern space-geodetic techniques (satellite laser ranging (SLR), very-long-baseline inter perometry (VLBI), global positioning system (GPS)) provide a present-day snapshot of the geological plate tectonic models and a picture of the present tectonic deformation. Several GPS networks have recently been set up for deformation studies along the Alpine–Himalayan collision zone in China (Wang et al. 2001), in the Eastern Mediterranean and Caucasus area (McClusky et al. 2000) or in the Alps (Vigny et al. 2002). In this context, Iran was a gap in the GPS data coverage of the Alpine–Himalayan collision zone. To fill this gap, Iranian and French research organizations started to set up several GPS networks in Iran. The largest GPS network covers most of the geological structures of Iran. It has been designed to measure the continental deformation within Iran and to determine

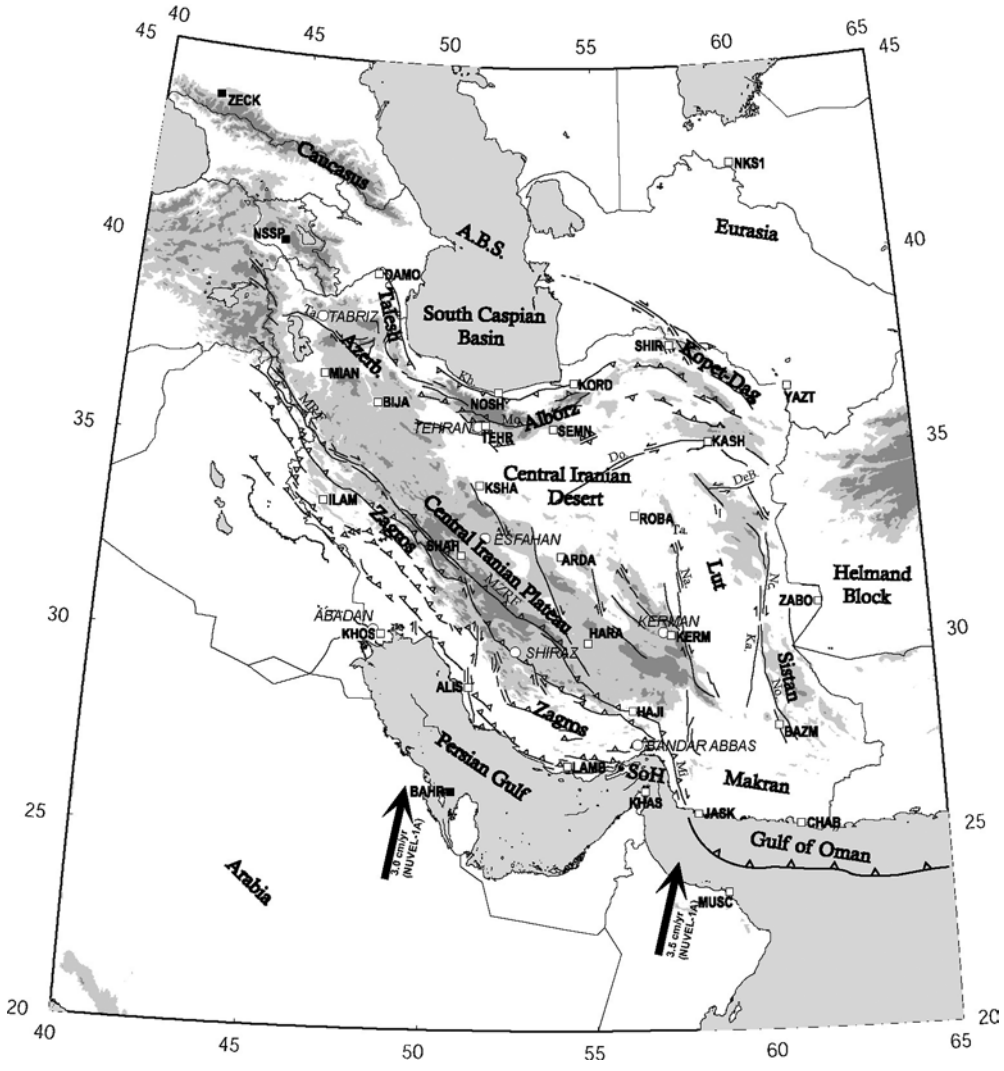

Fig. 1. Large-scale topographic map of the studied area. Iran is located between relatively undeformed shield areas to the southwest (Arabia) and northeast (Eurasia). The major structures are the mountain belts (Zagros, Makran, Talesh, Alborz, Kopet-Dag) and the stable areas (Azerbaijan, Central Iranian Desert, Lut block, South Caspian Basin). GPS sites are indicated by small squares (*white square* : French-Iranian network; *black square*: IGS station). *Small circles* represent the large cities. Azerb. = Azerbaijan; ABS = Apsheron–Balkhan Sill; Kh = Khazar Fault; Mo. = Mosha Fault; Ta. = Tabriz fault; MRF = Main Recent Fault; MZRF = Main–Zagros–Reverse Fault; Mi. = Minab-Zendan-Palami fault system; Do. = Doru-Doruneh Fault; DeB. = Dasht-e-Bayaz Fault; Ta. = Tabas Fault; Na. = Nayband Fault; Z = Zahedan Fault; Ne. = Neh Fault; Ka. = Kahurank Fault; No. = Nosratabad Fault

the relative part of each structure in the accommodation of the Arabia–Eurasia shortening. This article is devoted to the presentation of the first results obtained from the 1999 and 2001 GPS measurements.

2 Planning and measurement of the network

A GPS network of 28 sites with baselines of about 300 km in average has been installed in order to measure the velocity field in Iran (Fig. 1). Twenty-five sites are located in Iran, two in Oman and one in Uzbekistan. The spatial distribution of these sites is based on geological considerations. Each geological structure is covered by at least two sites in order to evaluate block rotations. Four stations, MUSC and KHAS in Oman and JASK and CHAB in the southeastern part of Iran, were specially planned to obtain the first direct velocity estimation of the subduction of the gulf of Oman beneath the Makran. The Alborz and Zagros belts are covered by four and six stations respectively. Only the Lut block is not covered, due to security problems. Some former GPS sites already installed in Iran have been reused in this project. This concerns in particular a large GPS network extended from Iran to the Pacific Ocean, the Asia–Pacific Regional Geodetic Project (APRGP, Matindas 1998). Five sites (ARDA, KASH, ZABO, CHAB, ALIS) from this network, were used. This will allow us to closely link the two geodynamic GPS projects in future analysis. Concrete pillars ($1.5 \times 1.5 \times 1.5$ m base and 1.5 m height above the base) were built to reduce site effects and centring errors. More than half of the sites are pillars (Table 1). The remaining sites are concrete benchmarks anchored in the bedrock. Tripods are used for the measurements of the latter sites.

The first GPS campaign was performed in September 1999. The 28 sites were measured with 18 dual-frequency receivers (nine Ashtech Z12 and nine Trimble 4000 SSI). Twenty-two sites were observed in two phases of four 24-hour sessions. The western part of the network was measured during DoY 259–262 and the eastern part during DoY 266–269. Three days were set for the transfer of the receivers and the observation teams between the two phases. Continuous measurements were made at the six remaining sites during the 11 days of the campaign (two sites in Oman, one site in Uzbekistan and three sites in Iran, see Table 1). These six sites allow us to link the two phases of measurements together. Choke-ring

Table 1. Availability of GPS data for the 1999 campaign. The last column indicates whether the site is a benchmark in the bedrock or a pillar

Site	Day of the year of GPS observations in 1999											Pillar
	259	260	261	262	263	264	265	266	267	268	269	
KHAS	X	X	X	X	X	X	X	X	X	X	X	N
MUSC	X	X	X	X	X	X	X	X	X	X	X	Y
NKS1		X	X	X	X	X	X	X	X	X	X	N
SHIR	X	X	X	X		X	X	X	X	X	X	Y
TEHR					X	X	X	X	X			Y
ZABO	X	X	X	X		X	X	X	X	X	X	Y
ALIS	X	X	X	X								Y
NOSH	X	X	X	X								Y
ARDA	X	X	X	X								Y
BIJA	X	X	X	X								Y
DAMO	X	X	X	X								Y
ILAM	X	X	X	X								Y
KHOS	X	X	X	X								Y
KSHA	X	X	X	X								N
SHAH	X	X	X	X								N
MIAN	X	X	X	X								Y
LAMB	X	X	X	X								N
YAZT								X	X	X	X	Y
BAZM								X	X	X	X	N
CHAB								X	X	X	X	Y
HAJI								X	X	X	X	Y
HARA								X	X	X	X	N
JASK								X	X	X	X	Y
KASH								X	X	X	X	Y
KERM								X	X	X	X	N
ROBA								X	X	X	X	Y
KORD								X	X	X	X	Y
SEMN								X	X	X	X	Y

antennas, which are the best available antennas for geodynamic studies, were used to reduce multipath and phase centre variation errors and to obtain the maximum precision. GPS-data sampling of 30 s and an elevation mask of 15°were set up. Due to well-trained observation teams and the use of good receivers, most of the expected data was actually gathered (Table 1). Raw data were transformed into RINEX format prior to processing.

The second GPS campaign was performed in October 2001. The whole network was measured, except NKS1 in Uzbekistan (due to security problems following the terrorist attacks in the USA). This second campaign was planned for the same time that the APRGP campaign ran, from DoY 281 to DoY 291. Therefore three new sites were added. The number of continuously recording stations during this second epoch increased in Iran (eight sites versus three) but decreased in the other countries (only one site in Oman). Once again the measurements were divided into two parts: a western part during DoY 281–284 (10 stations) and an eastern part during DoY 288–291 (11 sites). Thirty sites were surveyed during this second campaign and 27 were common with the first one. Table 2 shows the availability of GPS data for the second campaign.

3 Data processing

The GPS data analysis has been conducted using the GAMIT (version 10.05; King and Bock 2001) and GLOBK (version 10.0; Herring 2001) software in a three-step approach described by Feigl et al. (1993). In the first step, double-differenced GPS phase observations from each day were used to estimate station coordinates and the tropospheric zenith delay parameters at each station (13 parameters estimated by day). Loose a priori constraints were applied to all parameters and the ionosphere-free linear combination. We included in this analysis 19 IGS stations (BAHR, KIT3, POL2, ZECK, NICO, LHAS, ZWEN, BOR1, GILB, GLSV, GOPE, GRAZ, IRKT, JOZE, LAMA, PENC, POTS, RAMO, ZIMM) with positions and velocities well determined in ITRF2000 to serve as ties with the global reference frame. We used IERS (International Earth Rotation Service) Earth rotation parameters and applied azimuth-and elevation-dependent antenna phase-centre models, following the tables recommended by the IGS (Rothacher and Mader 1996). This daily solution enables us to clean the data. Each solution provides an independent estimation of the baseline components. Repeatabilities (i.e. the RMS of the daily independent measurements about their mean value) of these baseline components are a first indication of the quality of the data. For 1999, four strategies have been checked and compared (Fig. 2). Daily solutions were computed with (1) orbits adjusted and ambiguities fixed, (2) orbits adjusted and ambiguities free, (3) orbits fixed and ambiguities fixed, and (4) orbits fixed and ambiguities free. Statistics are shown in Table 3. The best repeatabilities are obtained for the first strategy, which has been adopted for the processing of the 1999 and 2001 data.

Part of Figs. 2 and 3 show the repeatabilities of baseline components for 1999 and 2001 obtained with

Table 2. Availability of GPS data for the 2001 campaign

Site	Day of the year of GPS observations in 2001											
	280	281	282	283	284	285	286	287	288	289	290	291
MUSC		X	X	X	X	X	X	X	X	X	X	
TEHN		X	X	X	X	X	X	X	X	X	X	X
ZABO		X	X	X	X	X	X	X	X	X	X	X
MASH	X	X	X	X	X	X	X	X	X	X	X	X
KASH	X	X	X	X	X	X	X	X	X	X	X	X
CHAB		X	X	X	X	X	X	X	X	X	X	
AHVA		X	X	X	X	X	X	X	X	X	X	X
ALIS	X	X	X	X	X	X	X	X	X	X	X	X
ARDA	X	X	X	X	X	X	X	X	X	X	X	X
TEHR		X	X	X	X							
KSHA		X	X	X	X							
LAMB		X	X	X	X							
MIAN		X	X	X	X							
NOSH		X	X	X	X							
SHAH		X	X	X	X							
BIJA		X	X	X	X							
ILAM		X	X	X	X							
DAMO		X	X	X	X							
KHOS		X	X	X	X							
BAZM									X	X	X	
HARA									X	X	X	X
JASK									X	X	X	X
KERM									X	X		
KHAS										X	X	X
KORD									X	X	X	X
ROBA									X	X	X	X
SEMN									X	X	X	X
SHIR									X	X	X	X
YAZT									X	X	X	X
HAJI											X	X

orbits adjusted and ambiguities fixed. They reach mean values of 1.1 mm (north component), 1.4 mm (east component) and 3.7 mm (vertical component) in 1999, and 0.9, 1.2 and 2.3 in 2001. The second campaign solution shows slightly better repeatabilities than the first one, which could be due to the use of three new permanent GPS stations (TEHN, MASH, AHVA, three stations common with Asia–Pacific survey at that time) and a better constellation of satellites in 2001. It is worth mentioning that the repeatabilities of stations with a tripod are nearly the same as those of stations with a pillar. This results from the careful calibration of the tribrachs before the campaign (which minimizes the centring errors) and the care of observers.

In the second step of the processing, we used the loosely constrained estimates of station coordinates and orbits and their covariances from each day as quasi-observation in a Kalman filter to estimate a consistent set of coordinates and velocities. In order to stabilize the solution we followed the strategy described by McClusky et al. (2000), who combine the daily solutions with SOPAC (Scripps Orbit and Permanent Array Center) daily solutions. We processed 15-day averaged estimates of 140 IGS station positions and covariances using the daily solutions performed at SOPAC (Bock et al. 1997; solutions available at http://lox.ucsd.edu). These 15-day averaged estimates from the beginning of 1995 to the end of February 2002 were combined with our survey solutions.

In the third step we applied generalized constraints (Dong et al. 1998) while estimating a six parameter transformation (six components of translation and rotation) in order to define a reference frame for our velocity estimates. First, horizontal velocity components were estimated in the International Terrestrial Reference Frame (ITRF2000) (Altamimi et al. 2002). We minimized the adjustment of the velocities of 31 high-quality geodetic stations used to define ITRF2000 (Altamimi et al. 2002) from a priori values given in the no-net-rotation (NNR) frame of ITRF2000. This produced a root mean square (RMS) departure of the velocities of the 31 stations after transformation of 0.5 mm/yr. Velocities obtained are shown in Fig. 4 and values given in Table 4. Second, a Eurasia-fixed reference frame was defined. Two alternatives were checked. First we rotated our estimated velocities in ITRF2000 to a Eurasian frame using the global plate model NUVEL-1A

Fig. 2. Baseline component repeatabilities versus baseline length for the 1999 campaign. First, second and third boxes are for north, east and vertical components. We have checked several strategies: orbits relaxed, ambiguities fixed; orbits fixed, ambiguities fixed; orbits relaxed, ambiguities free, orbits fixed, ambiguities free. The best repeatability is obtained for the first strategy

IRAN 1999 - IGS orbits relaxed - biases fixed

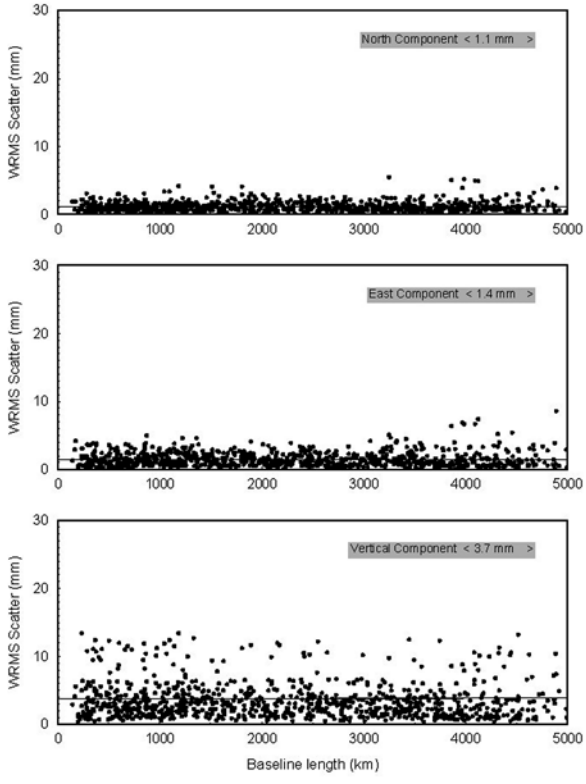

IRAN 1999 - IGS orbits - biases fixed

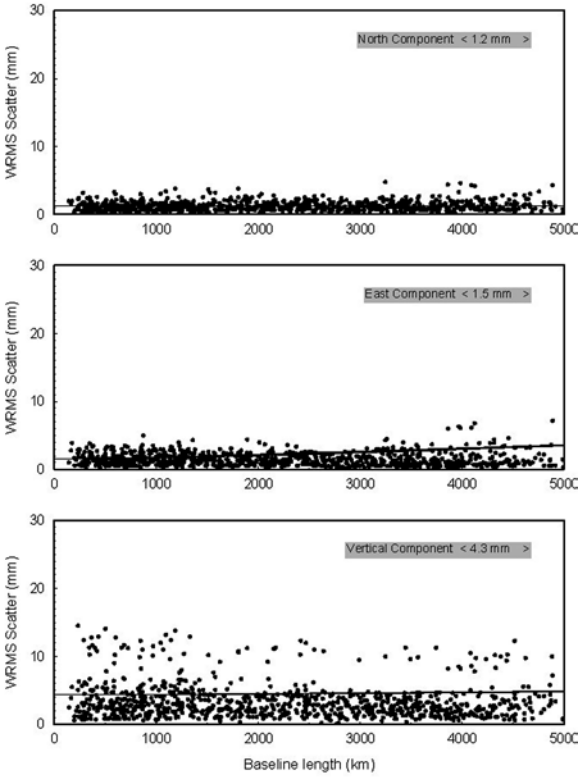

IRAN 1999 - IGS orbits relaxed - biases free

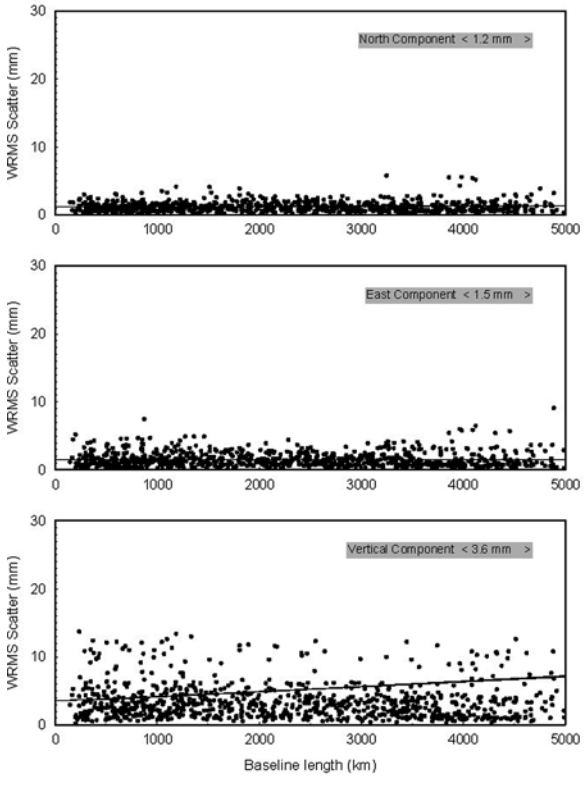

IRAN 1999 - IGS orbits - biases free

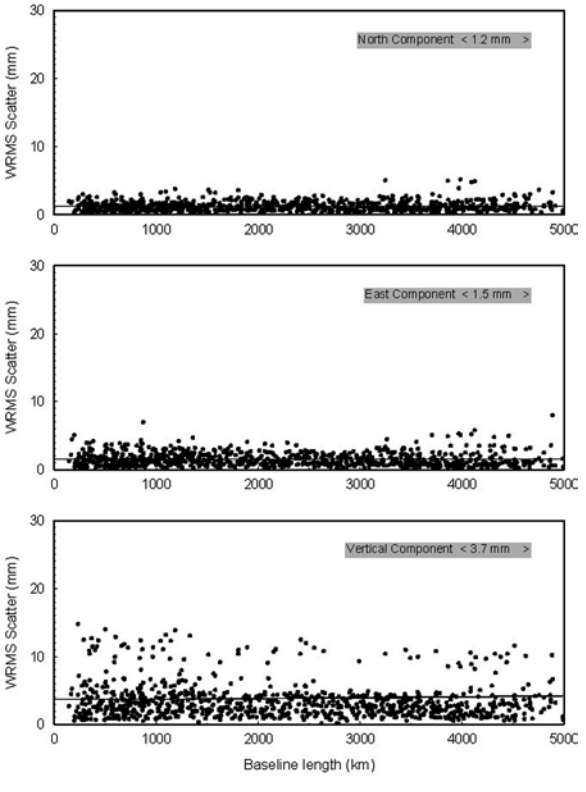

Table 3. Mean repeatabilities of baseline components for different solutions

Solution type	Mean repeatability (mm)		
	North	East	Up
1999 Re-estimated orbit			
Fixed ambiguity	**1.1**	**1.4**	**3.7**
Free ambiguity	1.2	1.5	3.6
IGS orbit			
Fixed ambiguity	1.2	1.5	4.3
Free ambiguity	1.2	1.5	3.7
2001 Re-estimated orbit			
Fixed ambiguity	**0.9**	**1.2**	**2.3**
Free ambiguity	1.1	1.4	3.7
IGS orbit			
Fixed ambiguity	1.0	1.5	2.9
Free ambiguity	1.2	1.8	4.3

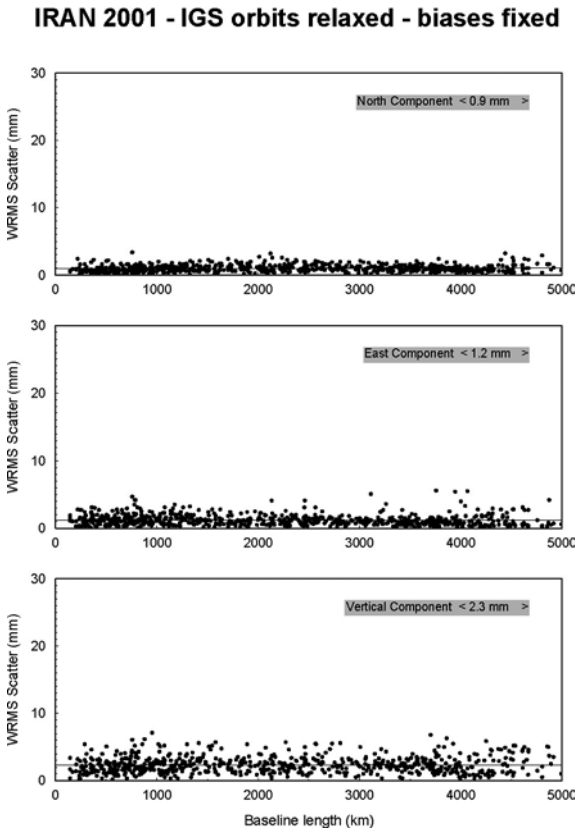

Fig. 3. 2001 baseline component repeatabilities versus baseline length. First, second and third boxes are for north, east and vertical components. The mean values are 1.1 mm (north component), 1.4 mm (east component) and 3.7 mm (vertical component) in 1999, and 0.9, 1.2 and 2.3 mm in 2001

(DeMets et al. 1994). The second alternative followed the approach described by McClusky et al. (2000). We minimized the horizontal velocities of 16 IGS stations in western Europe and central Asia (POL2, KIT3, ZWEN, METS, JOZE, TROM, BOR1, GRAZ, POTS, WTZR, ONSA, NYAL, ZIMM, KOSG, BRUS, HERS). The RMS departure of the velocities was 0.4 mm/yr. We rejected the first approach; though this solution produces a good global fit to ITRF2000, the residual velocity estimates for the stations used to define the stable Eurasia in the second alternative [following McClusky et al.'s approach (McClusky 2000)] after the rotation are too high (average of the absolute values of the residual velocities: east ~1.14 mm/yr, north ~2.16 mm/yr) in comparison with the second solution (east ~0.54 mm/yr, north ~0.68 mm/yr). This is probably due to a non-rigorous rotation pole predicted by NUVEL-1 A. Some differences between the rotation poles deduced from the ITRF2000 solution and the one predicted by NUVEL-1A have been notified by Altamimi et al. (2002). Velocities obtained are shown in Fig. 5 and values given in Table 5.

Obtaining good averages of the errors is not a trivial problem because different parameters must be considered. Error spectra of GPS data are spatially correlated because of common orbital, Earth rotation and regional atmospheric errors (Feigl et al. 1993). They are temporally coloured due to the time correlation of the errors from the atmospheric disturbance, monument instability and orbital misfits (Zhang et al. 1997; Mao et al. 1999). In order to produce an adequate representation of the uncertainties, we have adopted a non-rigorous approach described by McClusky et al. (2000). We weighted the data from each survey or set of continuous observations by averaging the increments in chi-square per degree of freedom from a forward and backward filtering of the data. We added a random walk component equal to 2 mm/yr to take into account the coloured noise and deal with a possible monument instability (Langbein and Johnson 1997). The uncertainties are given in Table 5 as one sigma standard deviation after scaling; in Figs 4 and 5 the plotted regions show 95% confidence.

A good agreement was found between our GPS velocities for some IGS stations (without constraints during the processing) and results of McClusky et al. (2000) and Wang et al. (2001). The resultant velocities for the common points of these two studies and our study are listed in Table 6. Conversely, it appeared that the velocities estimated for two sites (KHOS and HAJI in the south and southwest) were not consistent with the velocities estimated for the other sites (Fig. 5). These two sites indicated a large westward movement. Because the same antenna had been used for these two sites during the second campaign, it was strongly likely that the westward movement was due to technical problems. Fortunately these two sites were also recorded during two regional surveys performed in September 2001 in northern Zagros (KHOS) and January 2000 and January 2002 in the transition zone from Zagros to Makran (two common points with our survey, HAJI and JASK for reference). Therefore, we switched to use the data of the regional surveys, and we computed a new solution using the data from these two regional networks. The new velocity estimations solve the east velocity component problems for KHOS and HAJI. The new result obtained for JASK is consistent (about 1 mm/yr) with our first velocity estimation. An antenna calibration showed an offset in the east component of

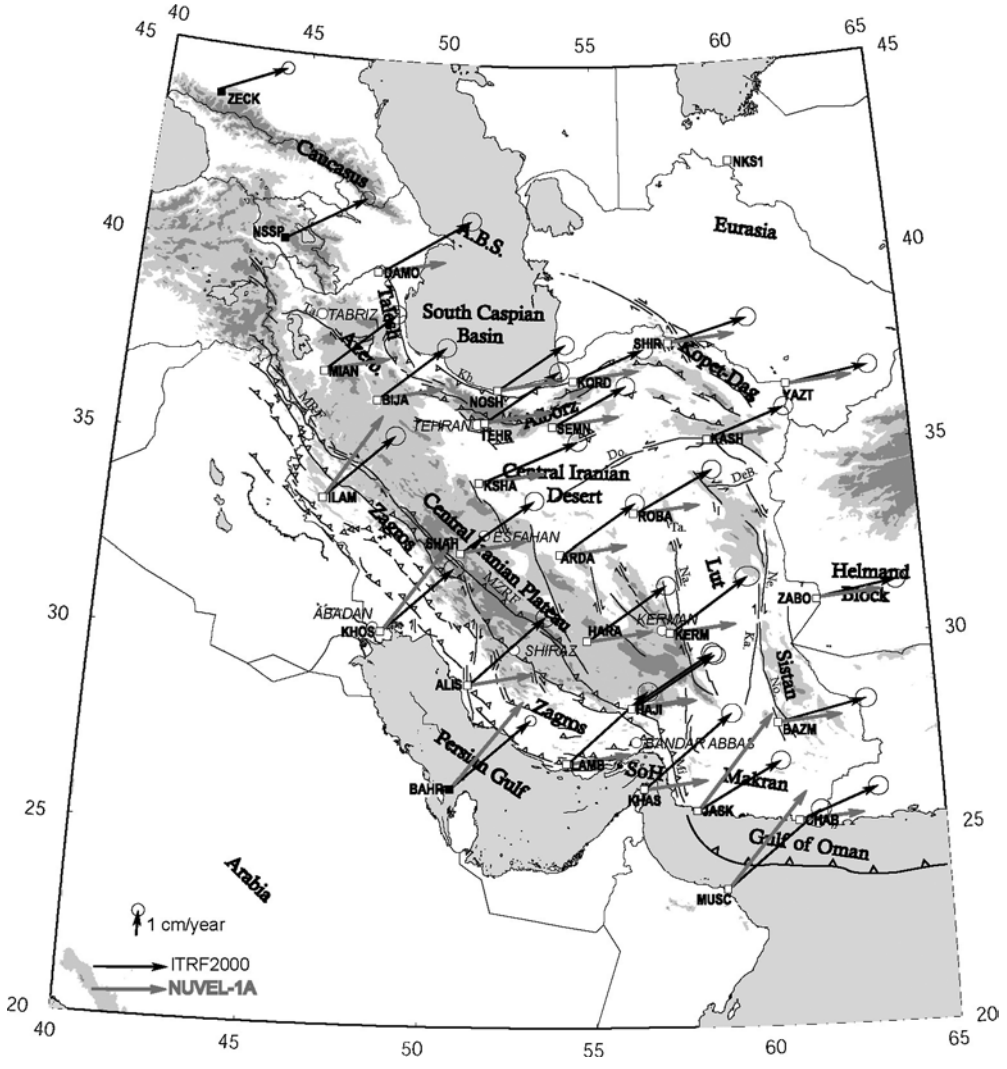

Fig. 4. Velocity obtained from GPS measurements calculated in ITRF2000 (black arrows) with their 95% confidence ellipse. *Grey arrows* indicate the values obtained for Nuvel-1A

-17.5 ± 1 mm. This result is consistent with the shift obtained between the first and second estimations (Fig. 5). The final coordinates and velocities are given in Table 5.

4 GPS velocity field

The velocity field in the ITRF2000 and the velocity field deduced from NUVEL-1A are shown in Fig. 4. A close correlation is observed between these two velocity fields in term of direction and magnitude for the sites located on the Arabian plate (MUSC, KHAS, BAHR, KHOS and ILAM) and for the two easternmost sites of the network (YAZT and ZABO) which are located on the stable Eurasia and the Helmand block respectively. Between these two sets of sites, the two velocity fields are not consistent: from the south to the east the observed velocity field is characterized by a progressive rotation from an azimuth of $\sim 45°$ to an azimuth of $\sim 85°$ while the NUVEL-1 A velocity field presents a sharp variation of the azimuth north of the northern boundary of the Arabian plate (Main Recent Fault and Main Zagros Reverse Fault). This is due to the definition of the NUVEL-1A model which is based on rigid plates. The computed velocity field clearly indicates that the transition from the stable Arabia to the stable Eurasia is not a sharp limit north of the Zagros but a broad region of about 2000 km.

Velocities in a Eurasia fixed reference frame following the McClusky et al. (2000) approach are shown in Fig. 5. Without a third measurement campaign, it is impossible to identify systematic errors and difficult to quantify the accuracy of our velocity field. Nevertheless, we observe a clear consistency in the velocity pattern for most stations. For example, the two stations HAJI located close together, show very similar displacements (within the 95% confidence range). Three sites show questionable results. The first one is NOSH, close to the Caspian sea. This site has a velocity which is not consistent with the velocity obtained in KORD 200 km to the east and with velocities obtained in the framework of another project, the Alborz GPS project. The Alborz GPS network contains 14 sites across the Alborz range. Preliminary results after two measurements in 2000 and 2001 give a velocity for MAHM located very close to NOSH of about 0.7 cm/year with an azimuth of about 340° (Masson et al. 2002). This result is more consistent

Table 4. Station positions and velocity estimations. Velocity values are those calculated in ITRF2000 (reference date 1997.0) and values obtained for NUVEL-1A. Plate are defined by the NUVEL-1A model. Velocities are given in mm/year

Site	Position		ITRF2000		NUVEL-1A		
	Long (°)	Lat (°)	E velocity	N velocity	E velocity	N velocity	Plate
ALIS	51.082	28.919	29.6	27.4	25.2	4.7	EURA
ARDA	53.822	32.313	28.9	20.6	25.5	3.9	EURA
BAHR	50.608	26.209	31.1	27.7	28.0	35.0	ARAB
BAZM	60.180	27.865	35.0	7.8	25.4	2.1	EURA
BIJA	47.930	36.232	25.8	21.8	25.4	5.6	EURA
CHAB	60.694	25.300	31.1	12.0	25.1	2.0	EURA
DAMO	47.744	39.513	34.5	22.3	25.3	5.6	EURA
HAJI	55.918	28.302	32.7	21.1	25.3	3.4	EURA
HARA	54.608	30.079	31.1	21.9	25.4	3.7	EURA
ILAM	46.427	33.648	26.6	25.5	21.1	33.1	ARAB
JASK	57.767	25.636	33.2	19.1	30.3	37.8	ARAB
KASH	58.464	35.293	30.2	11.4	25.8	2.6	EURA
KERM	57.119	30.277	30.5	21.7	25.5	3.0	EURA
KHAS	56.233	26.208	34.9	29.7	25.2	3.3	ARAB
KHOS	48.409	30.246	27.5	25.9	24.3	34.0	ARAB
KORD	54.199	36.860	27.4	12.2	25.7	3.8	EURA
KSHA	51.255	34.150	38.3	17.4	25.5	4.7	EURA
LAMB	54.004	26.883	31.8	28.6	25.1	3.9	EURA
MIAN	46.162	36.908	26.7	23.6	25.3	6.0	EURA
MUSC	58.569	23.564	37.4	30.7	31.8	38.1	ARAB
NOSH	51.768	36.586	25.8	18.4	25.6	4.5	EURA
ROBA	56.070	33.369	30.9	17.2	25.6	3.3	EURA
SEMN	53.564	35.662	28.2	16.0	25.6	4.0	EURA
SHAH	50.748	32.367	28.2	20.8	25.4	4.8	EURA
SHIR	57.308	37.814	30.9	9.1	25.8	3.0	EURA
TEHR	51.386	35.747	28.6	20.7	25.9	1.9	EURA
YAZT	61.034	36.601	32.7	5.4	25.9	1.9	EURA
ZABO	61.517	31.049	31.6	5.1	25.6	1.8	EURA

with the velocity of KORD and the expected result due to the tectonic shortening in the Alborz range. The offset is probably due to a site effect and not to an antenna motion relative to the pillar because NOSH has been measured with a forced centring device. Nevertheless, we cannot exclude that the velocity obtained for NOSH is due to tectonic displacements and not due to site problems. In this case the result suggests a large geological structure between NOSH and MAHM which has not been described by geologists. The second questionable site is KSHA. The results obtained in the sites neighbouring KSHA (SHAH and TEHR) display an azimuth of 350° ± 5°, while the azimuth of KSHA is 45° ± 5°. We have no way to control this site (no regional network) until the next survey. The third site is BAZM. For this site, it is strongly probable that the modulus of the velocity is very small (less than 5 mm/yr). Conversely, it is difficult to be confident in the azimuth, which seems to be inconsistent relative to the other velocity vectors. Therefore we prefer to wait for the third measurement before judging the validity of the result for KSHA and BAZM. The site of DAMO, close to Azerbaijan, also seems a little bit suspicious. In fact, the result obtained for DAMO is consistent in azimuth with the velocity of NSSP (Armenia). Moreover, the motion of DAMO seems to be compatible with unpublished GPS results in the easternmost Great Caucasus (Reilinger, pers. commun.). Finally, using MAHM instead of NOSH on the Caspian shoreline, a set of 26 points can be interpreted in terms of tectonic motion.

5 Discussion

Iran appears to be a key to understanding how the continental deformation is distributed during a young intra-continental collision. Our GPS study of this region improves the understanding of the mechanisms which govern the preliminary stages of major orogens.

5.1 Actual velocity of Arabia relative to Eurasia

The north–south shortening from Arabia to Eurasia is ~2.1 cm/year at the longitude of BAHR and ~2.5 cm/year at the longitude of MUSC (Fig. 6), less than previously estimated (NUVEL-1A: 3–3.5 cm/year). This is probably due to an oversimplification of NUVEL-1A. For example NUVEL-1A does not take into account the East African Rift. Adding this plate boundary, it is possible to define a new plate, the Somalian plate. This modifies slightly the velocity of the plates in the region (Jestin et al. 1994). This reduction of the Arabia–Eurasia velocity has to be taken into account in the quantification of the seismic/aseismic deformation ratio.

5.2 Eastern Iran: a velocity field resulting from oceanic subduction

The velocity of the subduction of the gulf of Oman beneath the Makran is ~1.8 cm/year in the east (from MUSC relative to CHAB) and decreases toward the

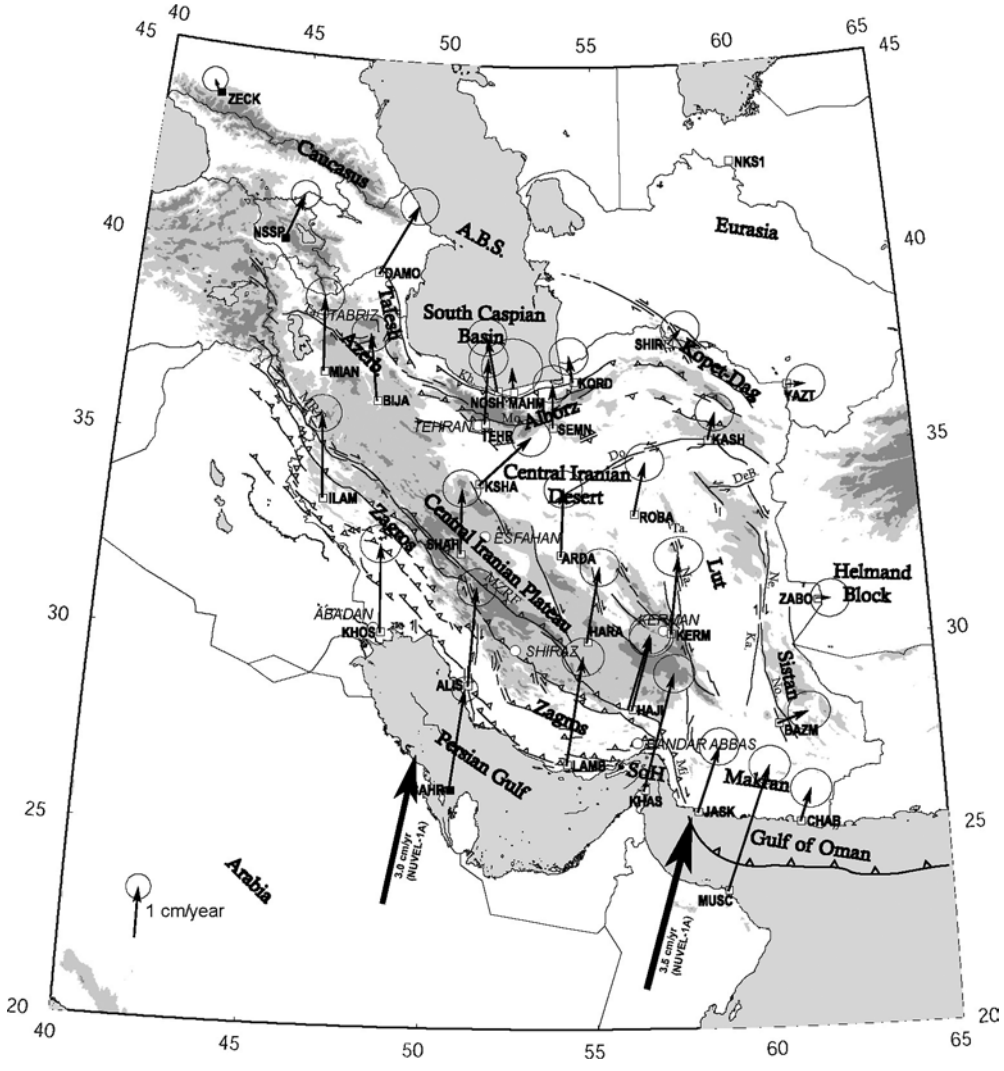

Fig. 5. GPS horizontal velocities and their 95% confidence ellipse in a Eurasia-fixed reference frame. *Grey arrows* in KHOS and HAJI indicate the velocities obtained using the initial data set. The final values have been obtained using data of regional networks (see text). The MAHM site has been added to control the validity of the NOSH velocity. The NOSH site is not consistent with the other sites of the same tectonic context (MAHM and KORD)

west (1.5 cm/year from MUSC relative to JASK). At the longitude of the Gulf of Oman, most of the Arabia–Eurasia shortening is located at the front of the subduction and in the Makran (see, for example, the velocity variation from MUSC relative to CHAB and BAZM). A large velocity variation is observed from the Central Iranian Desert to the Helmand block involving the Lut block. From KERM to ZABO the velocity variation is about 1.4 cm/year. The Lut block is a stable area surrounded by east–west left-lateral strike-slip faults in the north and north–south right-lateral strike-slip faults along its eastern and western limits. These faults allow the transition from the continental collision spread over the whole of western Iran (see below) to the stable Helmand block which does not move relative to Eurasia (velocity of ZABO close to 0) and is not included in the collision zone but considered as a stable area of Eurasia. This has been proposed already on the basis of the seismicity, which is very low in the Helmand block (Berberian et al. 2000, Ambraseys 2001). From the northern edge of the Lut block (KASH) to Eurasia (SHIR), the shortening seems to be small (about 0.3–0.4 cm/year). This results from the concentration of the deformation along the Makran subduction zone, as pointed out before.

5.3 Accommodation of the continental collision within the Zagros

In western Iran, the main feature of the continental collision is the Zagros range, which extends for about 1500 km along the NW–SE-trending boundary between the Arabian plate and Central Iran. The northern boundary of the Zagros is underlined by large faults orientated NW–SE, the Main Recent Fault (MRF) from the Turkish border to about SHAH and the Main Zagros Reverse Fault (MZRF) east of SHAH up to the Zagros–Makran transition zone (Berberian 1995). The dextral movement of the MRF accommodates the obliquity of the convergence between Arabia and Eurasia. Previous regional GPS results (Tatar et al. 2002) indicate a north–south shortening across the Zagros of about 1.0 cm/year.

The GPS velocity field indicates a very small shortening (0.1–0.2 cm/year) in the Persian Gulf. The shortening perpendicular to the Zagros axis decreases

Table 5. GPS site velocities and 1ó uncertainties with respect to the Eurasian-fixed reference frame. Longitude (Lon) and latitude (Lat) are given in degrees east and north, respectively. Station velocities and their uncertainties are given in mm/yr

Site	Long (°)	Lat (°)	E velocity	Eσ'[a]	N velocity	Nσ'[a]	Corr[b]
ALIS	51.082	28.919	1.3	1.6	19.6	1.5	0.02
ARDA	53.822	32.313	0.5	1.5	13.4	1.5	0.02
BAHR	50.608	26.209	2.6	1.1	20.0	1.0	0.04
BAZM	60.180	27.865	6.2	1.7	2.2	1.6	0.02
BIJA	47.930	36.232	−1.9	1.6	13.3	1.5	0.01
CHAB	60.694	25.300	2.4	1.7	6.5	1.5	0.02
DAMO	47.744	39.513	7.0	1.5	13.7	1.5	0.01
HAJI	55.918	28.302	4.1	1.8	14.4	1.5	0.03
HARA	54.608	30.079	2.6	1.6	14.9	1.5	0.02
ILAM	46.427	33.648	−1.2	1.6	16.6	1.5	0.01
JASK	57.767	25.636	4.6	1.6	12.8	1.5	0.02
KASH	58.464	35.293	1.6	1.6	5.4	1.5	0.02
KERM	57.119	30.277	1.9	2.0	15.3	1.6	0.03
KHAS	56.233	26.208	6.4	1.5	23.1	1.5	0.02
KHOS	48.409	30.246	−0.6	1.5	17.5	1.5	0.02
KORD	54.199	36.860	−0.8	1.5	5.2	1.5	0.02
KSHA	51.255	34.150	10.1	1.5	9.7	1.5	0.02
LAMB	54.004	26.883	3.3	1.5	21.5	1.5	0.02
MIAN	46.162	36.908	−0.9	1.5	14.7	1.5	0.01
MUSC	58.569	23.564	8.9	1.5	24.7	1.5	0.02
NOSH	51.768	36.586	−2.2	1.5	10.7	1.5	0.01
ROBA	56.070	33.369	2.4	1.5	10.6	1.5	0.02
SEMN	53.564	35.662	−0.1	1.5	8.8	1.5	0.02
SHAH	50.748	32.367	0.0	1.5	12.9	1.5	0.02
SHIR	57.308	37.814	2.5	1.5	2.8	1.5	0.02
TEHR	51.386	35.747	0.5	1.5	12.9	1.5	0.01
YAZT	61.034	36.601	4.0	1.5	0	1.5	0.02
ZABO	61.517	31.049	2.8	1.5	–0.1	1.5	0.02

[a] 1 sigma uncertainties
[b] Correlation coefficient between the east and north uncertainties

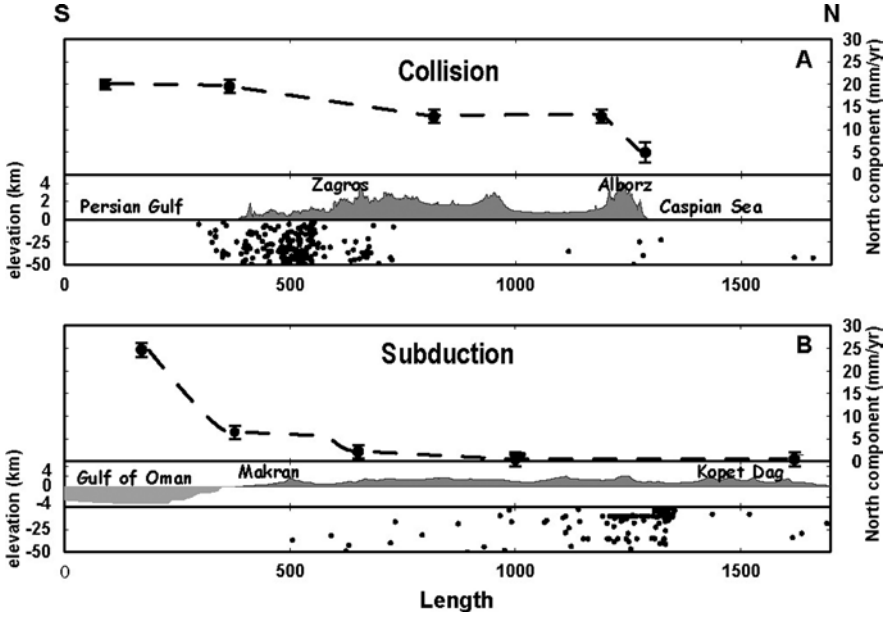

Fig. 6. North–south velocity along two profiles, together with the topography and the seismicity. **Top**: profile crossing the continental collision; **bottom**: profile crossing the subduction

from 0.6 cm/year in the Central Zagros (around Shiraz) to 0.3 cm/year in the Northern Zagros (around Ilam). Making the assumption that the partitioning to accommodate the oblique convergence is localized along the MZRF–MRF system, we obtain a right-lateral strike-slip movement decreasing from 0.5 cm/year in the Central Zagros to about 0.2 cm/year in the Northern Zagros. Based on geomorphology, higher values of 1.0–1.7 cm/year have recently been proposed (Talebian and Jackson 2002). Three causes could explain this discrepancy: (1) the overestimation of the Arabia–Eurasia motion inferred from the Nuvel-1A model, (2) the assumption that most of the strike-slip motion between Arabia and Eurasia is located along the MRF, and (3) the lack of absolute dating of geomorphic features. Despite its width and its proximity to the Arabian collider, the Zagros absorbs no more than 15–30% of the Arabia–Eurasia shortening.

The Zagros–Makran transition occurs around the Strait of Hormuz and is accommodated by a set of north–south faults located between Bandar-Abbas and

Table 6. Comparison of the velocities obtained in this study and other studies (McClusky et al. 2000, Wang et al. 2001) for some common IGS stations

Study	IGS Station	Position		Velocity	
		Lat (°)	Lon (°)	E Velocity	N Velocity
This study	IISC	77.570	13.021	14.0	32.6
Wang et al. (2001)	IISC	77.570	13.021	15.9	32.2
This study	LHAS	91.104	29.657	14.7	17.0
Wang et al. (2001)	LHAS	91.103	29.657	18.1	17.6
This study	NSSP	44.503	40.226	3.1	8.9
McClusky et al. (2000)	NSSP	44.5	40.226	3.6	8.1
This study	SHAO	121.200	31.100	3.5	−2.4
Wang et al. (2001)	SHAO	121.2	31.100	6.7	−4.9
This study	TAIW	121.537	25.021	10.1	−4.5
Wang et al. (2001)	TAIW	121.536	25.021	10.4	−3.0
This study	URUM	87.601	43.808	2.7	8.7
Wang et al. (2001)	URUM	87.705	43.808	3.7	6.6
This study	ZECK	43.79	41.56	−0.9	1.9
McClusky et al. (2000)	ZECK	43.79	41.56	0.5	0.8
This study	WUHN	114.357	30.532	3.7	−3.1
Wang et al. (2001)	WUHN	114.357	30.532	8.3	−4.6

Jask, the Minab–Zendan–Palami NNW–SSE fault system. The GPS velocity field indicates a right-lateral movement along the faults located in the Zagros–Makran transition zone of about 1.1 cm/year (from LAMB relative to JASK).

5.4 The northern pattern of the continental collision

As pointed out previously, the continental collision is not fully accommodated in the Zagros range, but spread out through a large zone which extends from the Sanandaj–Sirjan region up to the Greater Caucasus–Apsheron-Balkhan Sill–Kopet dag WNW–ESE line. This zone includes the Lesser Caucasus, the Talesh range, the South Caspian Basin and the Alborz range, the Azerbadjan and the Central Iranian Desert. The Sanandaj–Sirjan region and the Central Iranian Desert seem to accommodate a very small part of the shortening.

The Alborz is an east–west mountain range which accommodates shortening between the Central Iranian Desert and the south Caspian sea. From ARDA (Central Iranian Desert) to SEMN (south of the Alborz) and from SEMN to KORD (north of the Alborz), the NS shortening are respectively 0.4 and 0.4 cm/year. Making the assumption that most of the shortening in the Central Iranian Desert is located in the frontal thrusts south of Tehran, we can suggest that the total shortening through the Alborz is about 0.8 cm/year.

The Iranian Azerbadjan is located south of the Caucasus and west of the South Caspian Basin. This region is crossed by large NW–SE faults parallel to the Tabriz fault. The GPS velocity field indicates that the differential motion between the Sanandaj–Sirjan region (MIAN and BIJA) and the north of the Iranian Azerbadjan (DAMO) is large, and the residual strike-slip motion in a direction parallel to the Tabriz fault is on the order of 0.7 cm/yr. However, the precise distribution of the motion remains unknown.

The Greater Caucasus forms a high (4000–5000 m) but narrow (100–200 km) range which extends from the Black Sea to the Caspian Sea, where it dies out on the Apsheron peninsula. The deformation of the Greater Caucasus has already been studied by GPS (McClusky et al., 2000). Our results obtained for the IGS station in Armenia (NSSP) are consistent with these previous results (about 1.0 cm/year of shortening across the Lesser and the Greater Caucasus).

The eastward continuation of the Greater Caucasus beneath the Caspian Sea, the Apsheron–Balkhan Sill, is a prominent bathymetric feature separating the shallow northern Caspian Sea from the very deep South Caspian Basin. This structure is underlined by a dense and deep (more than 30 km depth, Priestley et al. 1994) seismicity which suggests a subduction of the south Caspian Sea beneath Eurasia along the Apsheron–Balkhan Sill (Jackson et al. 2002). Our result, based on MAHM and considering an undeformed South Caspian Basin, could indicate a subduction rate of about 0.5–0.6 cm/year. This rate is compatible with the velocity of 0.8–1.0 cm/year proposed by Jackson et al. (2002), taking into account that this rate is deduced from the overestimated NUVEL-1A Arabia–Eurasia shortening.

6 Conclusion

The precise distribution of the deformation in Iran was poorly constrained in the past as no geodetic measurements had previously been already performed. Now the deformation is better constrained. The north–south shortening from Arabia to Eurasia is ∼2.5 cm/year, less than previously estimated (Nuvel1 A: 3–3.5 cm/year). The velocity of the subduction of the Oman gulf beneath the Makran is ∼1.8 cm/year in the east and decreases toward the west. The transition from subduction (Makran) to collision (Zagros) is very sharp. In the eastern part of Iran, most of the shortening is accommodated in Makran, while in the western part the

shortening is more distributed from south (Zagros: ~0.8 cm/year) to north (Alborz: ~0.8 cm/year). The large faults around the Strait of Hormuz and the stable Lut block accommodate most of the subduction–collision transition (~1.4 cm/year). The Helmand block is fixed relative to Eurasia. The Kopet-Dag accommodates about 0.4 cm/year of shortening. Large right-lateral movement (~0.7 cm/year) seems to occur in the Tabriz region.

Acknowledgements. The Iran Global GPS project was sponsored by the National Cartographic Centre (NCC – Tehran), the French CNRS-INSU 'Intérieur de la Terre' programme, the International Institute of Earthquake Engineering and seismology (IIEES – Tehran). The GPS receivers were provided by CNRS-INSU and NCC. We would like to thank all the French and Iranian participants who helped during the fieldwork to make this study successful.

References

Altamimi Z, Sillard P, Boucher C (2002) ITRF2000: A new release of the International Terrestrial Reference Frame for Earth Science Applications. J Geophys Res: 107 doi: 10.1029/2001 JB000561

Ambraseys NN (2001) Reassessment of earthquakes, 1900–1999, in the Eastern Mediterranean and the Middle East. Geophys J Int 145:471–485

Berberian M (1995) Master blind thrust faults hidden under the Zagros folds: active basement tectonics and surface morphotectonics. Tectonophysics 241:193–224

Berberian M, Yeats RS (1999) Patters of historical earthquake rupture in the Iranian plateau. Bull Seism Soc Am 89:120–139

Berberian M, Jackson JA, Qorashi M, Talebian M, Khatib M, Priestley K (2000) The 1994 Sefidabeh earthquakes in eastern Iran: a blind thrusting and bedding-plane slip of growing anticline, and active tectonics of the Sistan suture zone. Geophys. J Int 142:283–299

Bock Y, Behr J, Fang P, Dean J, Leigh R (1997) Scripps Orbit and Permanent Array Center (SOPAC) and Southern Californian Permanent GPS Geodetic Array (PGGA). In: The global positioning system for the geosciences. National Academic Press, Washington, DC, pp 55–61

DeMets C, Gordon RG, Argus DF (1990) Current plate motions. Geophys J Int 101:425–478

De Mets C, Gordon RG, Argus DF, Stein S (1994) Effect of recent revisions to the geomagnetic reversal time scale on estimates of current plate motions. Geophys Res Lett 21:2191–2194

Dong T, Herring TA, King RW (1998) Estimating regional deformation from a combination of space and terrestrial geodetic data. J Geod 72:200–211

Feigl KL, Agnew DC, Bock Y, Dong D, Donnellan A, Hager BH, Herring TA, Jackson DD, Jordan TH, King RW, Larsen S, Larson KM, Murray MH, Shen Z, Webb F (1993) Space geodetic measurement of crustal deformation in Central and Southern California, 1984–1992. J Geophys Res 98:21,677–21,712

Herring TA (2001) Documentation for the GLOBK software version 9.5. Massachussetts Institute of Technology, Cambridge, MA

Jackson J, McKenzie D (1984) Active tectonics of the Alpine–Himalayan Belt between western Turkey and Pakistan. Geophys J Roy Astr Soc 77:185–264

Jackson J, Priestley K, Allen M, Berberian M (2002) Active tectonics of the South Caspian Basin. Geophys J Int 148:214–245

Jestin F, Huchon P and Gaulier JM (1994) The Somalia plate and the East African Rift System: present-day kinematics. Geophys J Int 116:637–654

King RW, Bock Y (2001) Documentation for the GAMIT GPS software analysis version 10.05, Massachussetts Institute of Technology, Cambridge, MA

Langbein J, Johnson H (1997) Correlated errors in geodetic time series: Implications for time-dependent deformation. J Geophys Res 102:591–603

Mao A, Harrison C, Dixon T (1999) Noise in GPS coordinate time series. J Geophys Res 104:2797–2816

Masson F, Sedighi M, Hinderer J, Bayer R, Nilforoushan F, Luck B, Vernant P, Chéry J, (2002) Present-day surface deformation and vertical motion in the Central Alborz (Iran) from GPS and absolute gravity measurements. European Geophysical Society Meeting, Nice, 21–26 April 2002

Matindas R (1998) The Status and Activity of the Working Group on Regional Geodetic Network of the Permanent committee on GIS Infrastructure for Asia and the Pacific workshop on regional geodetic network, Canberra, 2–4 July 1998

McClusky S, Balassanian S, Barka A, Demir C, Ergintav S, Georgiev I, Gurkan O, Hamburger M, Hurst K, Kahle H, Kastens K, Kekelidze G, King R, Kotzev V, Lenk O, Mahmoud S, Mishin A, Nadariya M, Ouzounis A, Paradissis D, Peter Y, Prilepin M, Reilinger R, Sanli I, Seeger H, Tealeb A, Toksoz M, Veis G (2000) Global positioning system constraints on plate kinematics and dynamics in the eastern Mediterranean and Caucasus. J Geophys Res 105:5695–5719

Priestley K, Baker C, Jackson J (1994) Implications of earthquake focal mechanism data for the active tectonics of the South Caspian Basin and surrounding regions. Geophys J Int 118:111–141

Rothacher M, Mader G (1996) Combination of antenna phase center offsets and variations: antenna calibration set $IGS_0$1. IGS Central Bureau/University of Berne, Switzerland

Talebian M, Jackson J (2002) Offset of the Main Recent Fault of NW Iran and implications for the late Cenozoic tectonics of the Arabia–Eurasia collision zone. Geophys J Int 150:422–439

Tatar M, Hatzfeld D, Martinod J, Walpersdorf A, Ghafori-Ashtiany M, Chéry J (2002) The present-day deformation of the central Zagros from GPS measurements. Geophys Res Lett 29(19), doi: 10.1029/2002 GLO15427

Vigny C, Chéry J, Duquesnoy T, Jouanne F, Ammann J, Anzidei M, Avouac JP, Barlier F, Bayer R, Briole P, Calais E, Cotton F, Duquenne F, Feigl K, Flouzat M, Gamond JF, Geiger A, Harmel A, Kasser M, Laplanche M, Le Pape M, Martinod J, Menard G, Meyer B, Ruegg JC, Scheubel JM, Scotti O, Vidal G (2002) GPS network monitors the Western Alps over a five year period: 1993–1998. Geodesy 76:63–76.

Wang Q, Zhang PZ, Freymueller JT, Bilham R, Larson KM, Lai X, You X, Niu Z, Wu J, Li Y, Liu J, Yang Z, Chen Q (2001) Present-day crustal deformation in China by global positioning system measurements. Science 294:574–577

Zhang J, Bock Y, Johnson H, Fang P, Williams S, Genrich J, Wdowinsky S, Behr J (1997). Southern California permanent GPS geodetic array: error analysis of daily position estimates and site velocities. J Geophys Res, 102:18,035–18,055